Coordination of Wind Farm and Pumped-Storage Hydro for a Self-Healing Power Grid

Amir Golshani [ID], *Member, IEEE*, Wei Sun, *Member, IEEE*, Qun Zhou, *Member, IEEE*,
Qipeng P. Zheng [ID], *Member, IEEE*, Jianhui Wang [ID], *Senior Member, IEEE*,
and Feng Qiu [ID], *Member, IEEE*

Abstract—The increasing penetration of wind energy poses great challenges to the operation of power systems in normal and emergency states. However, energy storage technologies can help accommodate wind power uncertainty and variability due to their flexible characteristics. This paper focuses on the restoration phase, and provides a novel coordination strategy of wind and pumped-storage hydro (PSH) units for a faster and reliable self-healing process. The wind-PSH assisted power system restoration is formulated as a two-stage adaptive robust optimization problem. The first-stage problem determines the start-up sequence of generators and the energization times of transmission paths; and the second-stage problem decides load pickup sequences, wind power dispatch levels, and PSH units' operating modes. The column-and-constraint generation decomposition algorithm is applied to solve the two-stage adaptive robust optimization problem, which has a mixed-integer optimization in the inner-level problem. The developed coordination strategy is tested on the modified IEEE 39-bus system. Numerical results demonstrate that the coordinated wind and PSH units can increase the total energy served, enhance wind power dispatchability, and reduce wind power curtailment.

Index Terms—Adaptive robust optimization, column-and-constraint generation, mixed-integer linear programming, pumped-storage hydro, self-healing, wind uncertainty.

NOMENCLATURE

Decision variables:

$u_{g,t}$	Binary variable equals to 1 if unit g is on at time t.
$u_{g,t}^{\text{start}}$	Binary variable equals to 1 if unit g is in start-up period at time t.
$u_{s,t}, u_{h,t}$	Binary variables equal to 1 if wind farm s and PSH unit h are on at time t.
t_g^{start}	Integer variable showing the start-up time of unit g.
$P_{g,t}$	Scheduled power of unit g at time t after connecting to the grid.
$P_{g,t}^{\text{start}}$	Start-up function of non-black-start unit g at time t before connecting to the grid.
$u_{b_n,t}$	Binary variable equals to 0/1 if bus n is de-energized/energized at time t.
$u_{k,t}$	Binary variable equals to 0/1 if line k is de-energized/energized at time t.
$P_{l,t}, Q_{l,t}$	Amount of real and reactive loads restored at load bus l and time t.
$P_{s,t}$	Scheduled power of wind farm s at time t.
$P_{h,t}, P_{h,t}^{\text{g(p)}}$	Net output power, generation/pumping power of PSH unit h at time t.
$q_{h,t}, q_{h,t}^{\text{g(p)}}$	Net water discharge, generation/pumping water discharge of PSH unit h at time t.
$P_{k,t}^{\text{flow}}, Q_{k,t}^{\text{flow}}$	Real and reactive power flows in line k at time t.
$R_t, R_{g,t}$	Total dynamic reserve and dynamic reserve share of unit g at time t.
$R_{l,t}, R_{h,t}$	Load shedding share of load bus l in dynamic reserve and dynamic reserve share of PSH unit h at time t.
$P_{s,t}^{\text{u}}$	Uncertain power of wind farm s at time t.
$I_{h,t}^{\text{g}}, I_{h,t}^{\text{p}}, I_{h,t}^{\text{I}}$	Binary variables indicating that hydro unit h is in generation, pumping, or idling mode at time t.
Vol_t	Volume of water stored in the reservoir at time t.

Constant parameters:

$P_g^{\max}, P_g^{\min}$	Maximum and minimum real power capacities of unit g.
$Q_g^{\max}, Q_g^{\min}$	Maximum and minimum reactive power capacities of unit g.
$Vol^{\max}, Vol^{\min}$	Maximum and minimum reservoir volume.
$q_h^{\max}, q_h^{\min}$	Maximum and minimum discharge rate of hydro unit h.
$P_h^{\min(\max),\text{g(p)}}$	Minimum/maximum power limit of PSH unit h in generation/pumping mode.
$\alpha_l, P_l^{\max}$	Priority factor and maximum restorable load at load bus l.

T_g, P_g^{start}	Start-up duration and cranking power of unit g.
λ_g	Maximum load pickup capability of generation unit g.
Δ_s	Budget of uncertainty related to wind farm s.
$\bar{P}_{s,t}, \widetilde{P}_{s,t}$	Forecasted power and the maximum forecast error of wind farm s at time t.

Sets:

G, T, L, L_{SH}	Sets of generators, restoration times, loads, and loads with under-frequency load shedding relays.
B, K, N_s, N_h	Sets of buses, transmission lines, wind farms, and PSH units.
$\mathcal{W}$	Uncertainty set for wind farm output power.

Indices:

b_n, b_m	Indices for buses at both ends of the lines.
b_g, b_l, b_s	Indices for generators, loads, and wind farms buses.
g, l, t, s, k, h	Indices for generators, loads, time periods, wind farms, lines, and PSH units.
w	Index for wind farm output power uncertainty realization.

I. INTRODUCTION

WIND energy is rapidly increasing worldwide. In the U.S., the total installed wind power capacity reached to over 60 GW at the end of 2012 [1]. Department of Energy has set the goal of achieving 20% of U.S. electricity from wind by 2030 [2]. However, the updated report shows that the wind power installed capacity has exceeded the level envisioned in 2008 [3]. As wind power is becoming a mainstream source of energy, its inherent variability and uncertainty present major concerns in power system operation and planning [4].

Operating wind power to achieve a self-healing power grid is particularly challenging. A self-healing process is initiated by system operators to mitigate cascading outages, or in the worst case, restore the system after a blackout [5]. A fast and reliable restoration procedure is essential to achieving the self-healing power grid. System operators re-start generating units, establish a transmission network, pick up customer loads, and eventually restore the system to normal condition. Wind variability and uncertainty can jeopardize system reliability throughout the restoration period. Most independent system operators (ISOs) are conservative on employing wind power for power system restoration. They either exclude wind energy resources from the restoration process or postpone their start-up times to the end. However, with the increasing penetration levels, exclusion of wind power will prolong the recovery time and leave the vast majority of loads unserved. Employing wind power in restoration is imperative and crucial. Also, accommodating wind uncertainty and variability is of a vital importance to a successful wind energy assisted restoration process.

Energy storage technologies are viable solutions to accommodate wind power uncertainty and variability due to their flexible characteristics. Among different storage technologies, pumped-storage hydro (PSH) is the most mature and economical option for large-scale applications. PSH units can switch between pumping and generation modes to provide fast-response energy and reserve. Coordinating with PSH units, wind energy resources will not impede, but rather, expedite the restoration process. An optimal coordination will minimize wind power curtailment (or spillage) during the restoration process, and hence a faster recovery can be achieved.

Research on employing wind power in system restoration is mainly focused on the operation and control of wind turbines [6]–[8]. In [6], different aspects of power system restoration together with constraints of wind farm restoration has been discussed. In [7], connecting a battery storage to the DC link capacitor of a doubly fed induction generator (DFIG) wind turbine resulted in black-start functionality. Offshore wind park connected to the HVDC link provided additional voltage control capability [8]. Firefly algorithm was used to find the optimal restoration plan with the aid of renewable sources [9].

Utilization of energy storages for expediting the distribution network restoration has been discussed in [10]–[12]. In [10], authors have studied the participation of plug-in hybrid electric vehicles (PHEVs) both as backup and storage units in the recovery process. It is shown that when PHEVs contribute as storage units, they could prevent congestion occurrence during the restoration period. In [11], we have adopted nonhomogeneous Markov chain method for generation of synthetic driving behavior of PHEV owners. It is shown that PHEVs could accelerate the load pickup process by compensating the imbalance between available generation and load. The benefits of utilizing distributed energy storages to support the distribution network restoration have been studied in [12].

In transmission level, dynamic model and simulation results of a black-start capable pumped-storage unit have been studied in [13]. The aforementioned literature have considered the participation of energy storages and wind generators independently. The coordination of wind and PSH units have also been studied, but only under normal operating conditions, such as economic dispatch and unit commitment problems [14], [15]. The study on the coordination of wind energy and PSH in emergency conditions is limited to date. We have proposed the idea of incorporating the renewable energy sources together with the energy storages in the power system restoration problem [16]. This paper expands on our previous work and tackles the wind-PSH coordination problem to expedite power system restoration. The coordination problem has been formulated as a two-stage combinatorial optimization problem and solved using an adaptive robust optimization approach. In the robust optimization, the probability function of uncertain parameters is unknown, and only an uncertainty set is defined based on the historical data or operator's experience.

The one-stage robust optimization approach was first introduced by Soyster [17] to handle parameter uncertainties in linear programming. As it provides the protection for all possible outcomes of the uncertain parameters, the solution could be overly conservative. For instance, if a wind farm participates in the restoration problem, one-stage optimization problem schedules an over-conservative plan for the conventional generators as it is considering the worst case realization of wind farm output power. In other words, it dispatches the conventional generators assuming that the wind farm output power will be deviated from

its scheduled power for the entire restoration period. As a result, one-stage restoration solutions prolong the restoration period. To this end, authors in [18] have proposed an approach to balance the robustness and total cost. Recently, more researchers have focused on the adaptive robust optimization and its application in management, business, and power systems [19], [20]. The proposed two-stage adaptive robust optimization alleviates the drawback of one-stage optimization method. That is, adaptive robust optimization considers increasing the dispatch levels of the conventional generators after it finds out the wind farm output power is not enough. In this way, the second-stage decisions of restoration problem will be made after the first-stage decisions are determined and the uncertainty of wind power is revealed. Thus, if the wind farm output power deviates from the forecasted value at restoration time t, the optimization problem will re-schedule the output power of the conventional units to compensate the power mismatch at time t.

Adaptive robust optimization models are usually transformed to multi-level optimization problems, which brings great challenges to the solution algorithms. In addition to approximation algorithms, decomposition-based algorithms have been proposed, especially for two-stage adaptive robust optimization, e.g., dual cutting planes [20], and column-and-constraint generation [21], [22]. In this paper, the column-and-constraint generation algorithm has been adopted to solve the two-stage adaptive robust optimization problem.

The major contributions of this paper are follows.
- Different stages of power system restoration process have been integrated in a holistic optimization problem. Constraints related to the wind farm, PSH units, and coordination between wind and PSH units are embedded into the restoration problem formulation.
- To deal with wind uncertainty, a two-stage adaptive robust optimization approach has been adopted. To overcome the computational burden, a decomposition algorithm, column-and-constraint generation (C&CG), is employed to solve the restoration problem.
- The developed coordination strategy enables system operators to fully utilize wind power with minimal wind spillage and take advantage of PSH units to expedite the restoration process.

The remainder of this paper is organized as follows. Section II introduces the wind-PSH coordination strategy in the power system restoration. Section III presents the power system restoration problem formulation using mixed-integer linear programming technique and adaptive robust optimization. In Section IV, the proposed strategy is examined under multiple case studies. Conclusions are provided in Section V.

II. WIND-PSH COORDINATION IN RESTORATION

After a blackout, power system operators work diligently to bring the system back to its normal state. System restoration consists of the following tasks: preparation and planning, black-start unit (BSU) start-up, transmission lines energization, non-black-start units (NBSUs) start-up, and load pickup [23].

Wind generators differ from conventional generators in two aspects: 1) they are intermittent and weather-dependent in
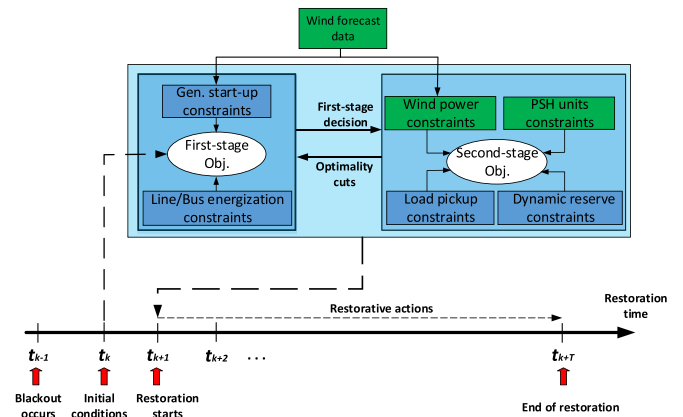
Fig. 1. Structure of two-stage wind-PSH assisted self-healing system.

nature; and 2) their output powers can highly fluctuate and cause large ramping events. PSH units can be employed to compensate wind power variability and uncertainty. The electricity absorbed or generated by PSH units needs to be coordinated to follow wind power profile. At times of high wind power generation, instead of curtailing, wind power can be harnessed to pump water from a lower reservoir and store in an upper reservoir. This usually occurs in the initial phase of restoration, when available online generators and transmission paths are limited. As the restoration progresses, the energy stored in the upper reservoir can be unleashed so that PSH units can participate in the restoration process. In case of wind power fluctuations, the stored water can be released to prevent frequency variations, causing load shedding or cascading outage at early stages of restoration. PSH units can handle wind uncertainty and expedite the recovery process. In this way, more wind power can be accommodated into the system which increases the headroom available on the conventional generators. Finally, PSH units can directly participate in load restoration and provide dynamic reserve if there is enough water already stored in the upper reservoir when the blackout occurs.

The structure of wind-PSH assisted restoration is depicted in Fig. 1. After a major contingency or blackout at t_{k-1}, the initial conditions of power grid are obtained at t_k to determine the extent of power outage. An optimal restoration plan is then devised with the aid of wind and PSH units and the restoration process starts at t_{k+1}. Wind uncertainty and variability as well as system reliability requirements are taken into account. In this paper, it is assumed that wind turbines are operated similar to a NBSU. That is, wind turbine can participate in restoration process after establishment of transmission paths. However, unlike conventional NBSUs, it has the capability of fast starting without demanding cranking power, and having fast ramping rate capability.

A two-stage adaptive robust optimization technique has been adopted. The first-stage objective is to maximize the total generation capacity, while the second-stage objective is to minimize the total unserved load [24]. In the first stage, start-up sequences of BSU, NBSUs, and wind generators as well as energization times of transmission paths are determined, given the generation and transmission constraints as well as wind farm

forecasted power. In the second stage, load pickup sequences, wind power dispatch levels, and operating modes of PSH units are determined, given the wind farm, PSH units, load pickup, and dynamic reserve constraints. The second-stage or dispatch decisions are made after observing the realization of wind farm output power. Note that the first-stage decisions are fixed when solving the second-stage problem. Once the worst case realization of the uncertainty is found, the optimality cut is generated and fed back to adjust the first-stage decisions. A detailed mathematical formulation of the proposed self-healing strategy is presented in the next section.

III. Two-Stage Robust Optimization

The objective function of restoration problem in the presence of wind and PSH units is to minimize the negative of the total generation capability and the total unserved load as expressed in (1) [24].

$$\min_{\Xi^{MP}} \sum_{t \in T} \sum_{g \in G} -(P_g^{\max} - P_g^{\text{start}})u_{g,t}$$
$$+ \max_{w \in \mathcal{W}} \min_{\Xi^{SP}} \sum_{t \in T} \sum_{l \in L} \alpha_l (P_l^{\max} - P_{l,t}) \quad (1)$$

In objective function (1), $P_g^{\max}$ and P_g^{start} are the maximum production level and cranking power of generator g, respectively. The binary decision variable $u_{g,t}$ denotes the status of generator g at restoration time t, i.e., 1 represents online and 0 offline. The decision variables pertaining to the first-stage (master) problem are in the set $\Xi^{MP} = \{u_{g,t}^{\text{start}}, u_{g,t}, t_g^{\text{start}}, P_{g,t}^{\text{start}}, u_{s,t}, u_{b,t}, u_{k,t}, u_{h,t}\}$. To ease and solve the restoration problem (1), we represent the problem in a two-stage way as shown in (1.1)–(1.3).

$$\min_{\Xi^{MP}} \sum_{t \in T} \sum_{g \in G} -(P_g^{\max} - P_g^{\text{start}})u_{g,t} + f(x) \quad (1.1)$$

In (1.1), x is a vector of the first-stage decisions and $f(x)$ is the recourse function showing the adaptive second-stage objective function under the worst case realization of uncertain parameter w. Function $f(x)$ is obtained from (1.2), where $g(x, w)$ is calculated in (1.3). In fact, objective function (1.3) is minimized under the worst case realization of uncertainty $w \in \mathcal{W}$ and first-stage decision x. In the second-stage objective function, $P_l^{\max}$ and $P_{l,t}$ are the maximum restorable active load and the amount of restored active load, respectively, at load bus l and restoration time t. The load priority is denoted as α_l. The decision variables pertaining to the second-stage problem are the elements of the set $\Xi^{SP} = \{P_{g,t}, P_{l,t}, Q_{l,t}, P_{s,t}, P_{h,t}, q_{h,t}, P_{k,t}^{\text{flow}}, Q_{k,t}^{\text{flow}}, P_{s,t}^{\text{u}}, I_{h,t}^{\text{g}}, I_{h,t}^{\text{p}}, I_{h,t}^{\text{l}}, R_t, R_{g,t}, R_{h,t}, R_{l,t}, Vol_t\}$.

$$f(x) = \max_{w \in \mathcal{W}} g(x, w) \quad (1.2)$$

Where,

$$g(x, w) = \min_{\Xi^{SP}} \sum_{t \in T} \sum_{l \in L} \alpha_l (P_l^{\max} - P_{l,t}) \quad (1.3)$$

A number of constraints are taken into account to address the restoration process as well as wind-PSH coordination. All decision variables satisfy $\forall t \in T$, $\forall g \in G$, $\forall k \in K$, $\forall (b_g, b_s, b_l, b_h, b_n, b_m) \in B$, $\forall l \in L, s \in N_s, h \in N_h$.

A. First-Stage Constraints

1) Initial Conditions: System operators can set the initial conditions based on system status and the extent of outage. In this paper, we assume a complete blackout condition and constraints (1.4)–(1.6) represent the initial conditions of generation units, transmission lines and buses, respectively.

$$u_{g,t=0}^{\text{start}} = 0 \quad (1.4)$$

$$u_{k,t=0} = 0 \quad (1.5)$$

$$u_{b_n,t=0} = 0 \quad (1.6)$$

Constraint (1.7) forces the BSU to get started at $t = 1$.

$$u_{g,t=1}^{\text{start}} = 1, \quad g \in G_{\text{BSU}} \quad (1.7)$$

2) Generator Start-Up Function: The start-up characteristic of NBSUs is shown in (1.8), where integer variable t_g^{start} and parameter T_g represent start-up and cranking times, respectively. P_g^{start} is the cranking power of generator g.

$$P_{g,t}^{\text{start}} = \begin{cases} 0 & 0 < t < t_g^{\text{start}} \\ P_g^{\text{start}} & t_g^{\text{start}} \le t \le t_g^{\text{start}} + T_g \end{cases} \quad (1.8)$$

3) Energization Constraints: Units need to be started; buses and lines need to be energized. Their energization statuses are inherently correlated. Constraint (1.9) shows that each NBSU's start-up sequence is initiated only after the energization of its respective bus, b_g. Binary variable $u_{g,t}$ can be derived from (1.10). As a NBSU, wind farm cannot participate until its bus b_s is energized in (1.11). Also, PSH units can contribute only after the energization of their respective buses in (1.12). Assuming that a transmission line k connects buses n and m, if both buses are de-energized at restoration time t, then the transmission line k is de-energized at time t in (1.13). In (1.14), a transmission line k can be energized one restoration time unit after the energization of one of its connected buses.

$$u_{g,t}^{\text{start}} \le u_{b_g,t} \quad (1.9)$$

$$\sum_{t \in T}(1 - u_{g,t}) \ge \sum_{t \in T}(1 - u_{g,t}^{\text{start}}) + T_g \quad (1.10)$$

$$u_{s,t} \le u_{b_s,t} \quad (1.11)$$

$$u_{h,t} \le u_{b_h,t} \quad (1.12)$$

$$u_{k,t} \le u_{b_{n(m)},t} \quad (1.13)$$

$$u_{k,t+1} \le (u_{b_n,t} + u_{b_m,t}) \quad (1.14)$$

B. Second-Stage Constraints

1) Power Balance Constraints: Electricity generation and load should be balanced at all times. For generators, the real and reactive power outputs should be bounded by their capacities,

denoted in constraints (1.15) and (1.16). Nodal active and reactive power balances are shown in (1.17) and (1.18), respectively. Where, $P_{k,t}^{\text{flow}}$ and $Q_{k,t}^{\text{flow}}$ are active and reactive power flows of line k in restoration time t, respectively. We adopted the linear form of ACOPF proposed in [25] to compute $P_{k,t}^{\text{flow}}$ and $Q_{k,t}^{\text{flow}}$.

$$P_g^{\min} u_{g,t} \leq P_{g,t} \leq P_g^{\max} u_{g,t} \tag{1.15}$$

$$Q_g^{\min} u_{g,t} \leq Q_{g,t} \leq Q_g^{\max} u_{g,t} \tag{1.16}$$

$$\sum_{g \in G}(P_{g,t} - P_{g,t}^{\text{start}}) + \sum_{s \in N_s} P_{s,t} + \sum_{h \in N_h} P_{h,t} - \sum_{l \in L} P_{l,t}$$

$$= \sum_{k \in K} P_{k,t}^{\text{flow}} \tag{1.17}$$

$$\sum_{g \in G} Q_{g,t} + \sum_{s \in N_s} Q_{s,t} - \sum_{l \in L} Q_{l,t} = \sum_{k \in K} Q_{k,t}^{\text{flow}} \tag{1.18}$$

2) Load Pickup and Dynamic Reserve Constraints: The maximum load pickup capability at each restoration time has a direct relationship with the inertia of generation units and turbine-governor models. One method to address this important issue in the restoration problem is to integrate frequency response equations into the second-stage problem. However, the time frame of interest in dynamic analysis is remarkably smaller than the time frame of the restorative actions proposed in the literature (e.g. 5 or 10 minutes). There are two approaches that have been widely adopted in the literature to cope with this issue and make sure that the minimum frequency (nadir) constraint will not be violated after a load pickup action.

The first approach is to derive a linear constraint that relates the load pickup size to frequency nadir, inertia, and governor characteristics, as presented in [24]. The second approach to calculate the load pickup size and dynamic reserve has been proposed in [26] and adopted in this paper. This approach defines a load pickup factor for each generation unit. That is, the maximum load that a generator can pick up is calculated as a percentage of generator rating without causing a drop in frequency below the safe operating level (e.g. 59.5 Hz). These so called "Rule of Thumb" load pickup factors are 5% for fossil steam, 15% for hydro, 25% for combustion turbines. Then, the total load pickup capability is the summation of load pickup capability of all online generation units at each restoration time. Load can be picked up right after the energization of its corresponding bus u_{b_l} in (1.19). The maximum load pickup capability is restricted in (1.20). In (1.21), λ_g shows the load pickup capability of generator g in each restoration time interval, which is assumed to be 25% for combustion (CT) and PSH units, and 5% for steam turbines (ST).

Dynamic reserve consists of the reserve on generator that is available via generator governor action, and loads with under-frequency load shedding (UFLS) relays [26]. The amount of dynamic reserve needed can be computed by knowing the load pickup factors of paralleled units at each restoration time. It should be noted that the maximum level of dispatch for a generation unit, or in other words, the largest energy contingency, should not exceed the maximum available dynamic reserve at each restoration time. Otherwise, the remaining generators in

the system could not maintain acceptable frequency after the trip of that generator. In (1.22), the total dynamic reserve is calculated for each restoration time and it is assumed that PSH units can also contribute to dynamic reserve. Output power of generators should be enforced in (1.23) to maintain system security. In (1.24), it is assumed that less than 50% of dynamic reserve in the system should be devoted to the loads with under-frequency load shedding relays, according to the recommendation in [26]. The aforementioned constraints ensure that the minimum frequency never goes below 59.5 Hz after the largest contingency. However, after surviving the contingency, the AGC or synchronous reserve should kick in and bring the frequency back to its nominal value. Note that this paper has not accounted for the secondary control actions that might be taken to restore the frequency to its pre-contingency value.

$$0 \leq P_{l,t} \leq P_l^{\max} u_{b_l,t} \tag{1.19}$$

$$\sum_{l \in L} P_{l,t+1} - \sum_{l \in L} P_{l,t} \leq \sum_{g \in G} R_{g,t} + \sum_{h \in N_h} R_{h,t} \tag{1.20}$$

$$R_{g,t} \leq \min\left(P_g^{\max}\lambda_g, P_g^{\max} - P_{g,t}\right) \tag{1.21}$$

$$R_t \leq \sum_{l \in L_{SH}} R_{l,t} + \sum_{g \in G} R_{g,t} + \sum_{h \in N_h} R_{h,t} \tag{1.22}$$

$$P_{g,t} \leq R_t - R_{g,t} \tag{1.23}$$

$$\sum_{l \in L_{SH}} R_{l,t} \leq 0.5 R_t \tag{1.24}$$

3) Wind Farm Constraints: Wind farm power curtailment is allowed in constraint (1.25). Part of wind farm power that is participating in the load pickup should satisfy the dynamic reserve and excess wind energy is used to pump water to an upper reservoir in constraint (1.26).

$$P_{s,t} \leq P_{s,t}^{\text{u}} u_{b_s,t} \tag{1.25}$$

$$\sum_{s \in N_s} P_{s,t} - \sum_{h \in N_h} P_{h,t}^{\text{p}} \leq R_t \tag{1.26}$$

4) Uncertainty Set: In this paper, a polyhedral uncertainty set $\mathcal{W}$ is adopted and defined in (1.27). It contains wind power forecast $\bar{P}_{s,t}$ along with the maximum forecast error $\widetilde{P}_{s,t}$, showing its deviation from the forecasted value. As the uncertainty bound increases, the size of uncertainty set enlarges and the resulting solutions become more conservative. In (1.27), Δ_s is the budget of uncertainty and controls the total deviation of wind farm output power from the forecasted value. Δ_s can take value between 0 and T, for instance, $\Delta_s = 0$ corresponds to the least conservative case in which $P_{s,t}$ is forced to be its forecasted value.

$$\mathcal{W} := \left\{ P_{s,t}^{\text{u}} \in \mathbb{R}^{|N_s| \times |T|} : \sum_{t \in T} \frac{\left|P_{s,t}^{\text{u}} - \bar{P}_{s,t}\right|}{\widetilde{P}_{s,t}} \leq \Delta_s, \right.$$

$$\left. P_{s,t}^{\text{u}} \in \left[\bar{P}_{s,t} - \widetilde{P}_{s,t}, \bar{P}_{s,t} + \widetilde{P}_{s,t}\right] \; \forall s \in N_s \right\} \tag{1.27}$$

5) PSH Constraints: Generally, output power of a hydro unit is a non-linear non-convex function of the turbine discharge rate

and the net head [27]. In this paper, variations on the net water head are neglected, and it is assumed that each PHS unit has one water-to-power curve for the generation mode and one power-to-water curve for the pumping mode [15]. The difference between two curves is defined as PSH efficiency. Their piecewise-linear approximations are obtained by using auxiliary binary variables similar to the method presented in [27]. In (1.28), binary variables $I_{h,t}^{g}$, $I_{h,t}^{p}$, $I_{h,t}^{I}$ indicate that hydro unit h is in generation, pumping, or idling mode, and theses modes are mutually exclusive in each restoration time t. Reservoir volume limits are shown in constraint (1.29). Reservoir volume relationship with PSH discharge rate is shown in constraint (1.30). In (1.31), the net output power of PSH unit h is computed. Constraints (1.32)–(1-35) are applied to both pumping (p) and generation (g) modes. Where, $P_{h,t}$ shows the output power and $q_{h,t}$ is the water discharge rate of PSH unit h. The generation and pumping mode capacity limits are satisfied in (1.32)–(1.35).

$$I_{h,t}^{g} + I_{h,t}^{p} + I_{h,t}^{I} \leq 1 \qquad (1.28)$$

$$Vol^{\min} \leq Vol_t \leq Vol^{\max} \qquad (1.29)$$

$$Vol_{t+1} = Vol_t - q_{h,t}\Delta T \qquad (1.30)$$

$$P_{h,t} = P_{h,t}^{g} - P_{h,t}^{p} \qquad (1.31)$$

$$q_h^{\min} u_{b_h,t} \leq q_{h,t}^{p(g)} \leq q_h^{\max} u_{b_h,t} \qquad (1.32)$$

$$P_h^{\min,p(g)} u_{b_h,t} \leq P_{h,t}^{p(g)} \leq P_h^{\max,p(g)} u_{b_h,t} \qquad (1.33)$$

$$q_h^{\min} I_{h,t}^{p(g)} \leq q_{h,t}^{p(g)} \leq q_{h,t}^{\max} I_{h,t}^{p(g)} \qquad (1.34)$$

$$P_h^{\min,p(g)} I_{h,t}^{p(g)} \leq P_{h,t}^{p(g)} \leq P_h^{\max,p(g)} I_{h,t}^{p(g)} \qquad (1.35)$$

C. Solution Algorithm

The wind-PSH assisted restoration is a two-stage adaptive robust optimization problem with mixed-integer recourse. We adopt C&CG decomposition algorithm as the solution methodology [21], [22]. The two-stage restoration problem (1.1)–(1.35) can be written in the following compact matrix form:

$$\min_{\boldsymbol{x} \in \{0,1\}^n} \boldsymbol{c}^T \boldsymbol{x} + \max_{\boldsymbol{\omega} \in \mathcal{W}} \min_{\boldsymbol{y},\boldsymbol{z} \in \Omega(\boldsymbol{x},\boldsymbol{\omega})} \boldsymbol{b}^T \boldsymbol{y} \qquad (2.1)$$

$$\text{s.t.} \quad \boldsymbol{F}\boldsymbol{x} \leq \boldsymbol{f} \qquad (2.2)$$

$$\Omega(\boldsymbol{x},\boldsymbol{\omega}) = \{\boldsymbol{B}\boldsymbol{y} + \boldsymbol{Q}\boldsymbol{z} \leq \boldsymbol{g} - \boldsymbol{A}\boldsymbol{x} - \boldsymbol{H}(\boldsymbol{\omega})\boldsymbol{x}$$

$$\boldsymbol{\omega} \in \mathcal{W}, \ \boldsymbol{y} \in \mathbb{R}, \ \boldsymbol{z} \in \{0,1\}^m \} \qquad (2.3)$$

Where $\boldsymbol{F}$, $\boldsymbol{B}$, $\boldsymbol{Q}$, and $\boldsymbol{A}$ are constant coefficient matrices, whereas, $\boldsymbol{H}(\boldsymbol{w})$ is an uncertainty dependent coefficient matrix. Binary variable vector $\boldsymbol{x}$ represents the first-stage decisions, continuous variable vector $\boldsymbol{y}$ and binary variable vector $\boldsymbol{z}$ represent the second-stage decisions. Now, we apply nested C&CG to decompose (2.1)–(2.3) to a master problem with an outer-level C&CG algorithm and a MILP subproblem with an inner-level C&CG algorithm. The detailed description of the outer-level and inner-level algorithms can be found in the Appendix.
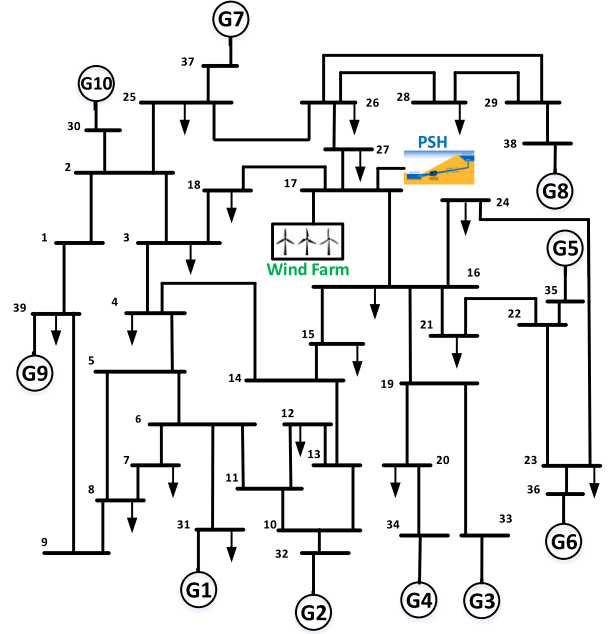
Fig. 2. Modified IEEE 39-bus system.

TABLE I
PSH UNITS' CHARACTERISTICS

Parameter	Value	Parameter	Value
$q_h^{\min}$	0.05 (Hm^3/hr)	$P_h^{\min,p}$	20 (MW)
$q_h^{\max}$	0.75 (Hm^3/hr)	$P_h^{\max,p}$	250 (MW)
$P_h^{\min,g}$	16 (MW)	$Vol^{\max}$	10 (Hm^3)
$P_h^{\max,g}$	180 (MW)	$Vol^{\min}$	3 (Hm^3)

TABLE II
GENERATORS' CHARACTERISTICS

Gen No.	$P_g^{\min}$ (MW)	$P_g^{\max}$ (MW)	$Q_g^{\min}$ (MVar)	$Q_g^{\max}$ (MVar)	P_g^{start} (MW)
1	0	570	-200	300	5
2	0	650	-250	300	7
3	0	630	-250	250	5
4	0	600	-220	300	8
5	0	650	-200	300	6
6	0	560	-200	200	6
7	0	560	-200	200	6
8	0	830	-300	300	7
9	0	1100	-400	500	8
10	0	250	-150	150	0

IV. NUMERICAL RESULTS

A modified IEEE 39-bus system has been adopted for testing. The system contains 10 generators, a 600 MW wind farm located at bus 17, and two PSH units, as shown in Fig. 2. The characteristics of PSH units are given in Table I. The generators' characteristics are given in Table II. The load values and priority factors are indicated in Table III. Coefficient α_l in the objective function is critical to guarantee the power supply to the high priority customers. Two cases, low and high wind power fluctuations, are considered to examine the effectiveness of wind-PSH

TABLE III
LOAD VALUES AND PRIORITIES

Bus	P_l^{max} (MW)	Priority	U/f relay	Bus	P_l^{max} (MW)	Priority	U/f relay
3	322	1.0	No	21	274	0.9	No
4	500	0.8	Yes	23	247	0.8	Yes
7	233	1.0	No	24	308	1.0	No
8	522	1.0	No	25	224	0.9	No
12	7.5	1.0	No	26	139	1.0	No
15	320	0.8	Yes	27	281	1.0	No
16	329	1.0	No	28	206	0.9	No
18	185	0.9	No	31	9.2	1.0	No
20	680	1.0	No	39	1100	1.0	No

TABLE IV
GENERATORS' OPTIMAL ON TIMES AND TYPES

Gen. No.	Bus No.	Time (p.u.)	Type unit	Gen. No.	Bus No.	Time (p.u.)	Type unit
G1	31	12	CT	G6	36	14	CT
G2	32	13	ST	G7	37	9	CT
G3	33	13	ST	G8	38	15	ST
G4	34	14	ST	G9	39	14	ST
G5	35	14	ST	G10	30	2	CT

coordination in the restoration process. In both cases, the base power is 100 MW and each restoration time step is 10 minutes (1 p.u.) for preparation and stabilization. The characteristics of buses, transmission lines are taken from [28]. The confidence interval of wind farm output power is set as 10% of the forecasted value. The proposed C&CG algorithm is implemented in C++ using ILOG CPLEX 12.6 and the Concert Library. All simulations were executed on a PC with Intel CoreTM i5 CPU @3.30 GHz and 8 GB RAM.

A. Base Case: Perfect Forecast Without PSH Units

An illustrative example with perfect wind forecast data is presented to investigate the wind spillage phenomenon. Energy storage is not considered in the example. Neglecting wind uncertainty, the optimization problem (1.1)–(1.35) turns to a deterministic MILP problem. Table IV summarizes generators' online times. G10 is the BSU with a self-starting capability which becomes online at $t = 2$. The forecasted and scheduled wind power is depicted for the early stages of restoration in Fig. 3. Note that before restoration time $t = 5$, the wind farm generates zero power. Subsequently, wind farm output power increases slightly, with a large portion curtailed. Finally, at $t = 12$ all wind power is utilized in the restoration process. The total energy served is 11.70 GWh and total wind energy spillage is 631.75 MWh.

The area between two curves can be divided into two regions separated by a red dashed line: Area 1 represents the amount of wind energy that is spilled due to the unavailability of transmission path, and Area 2 represents the amount of wind energy that is curtailed to maintain power system security. In fact, wind energy spillage in area 2 can be reduced using energy storage.
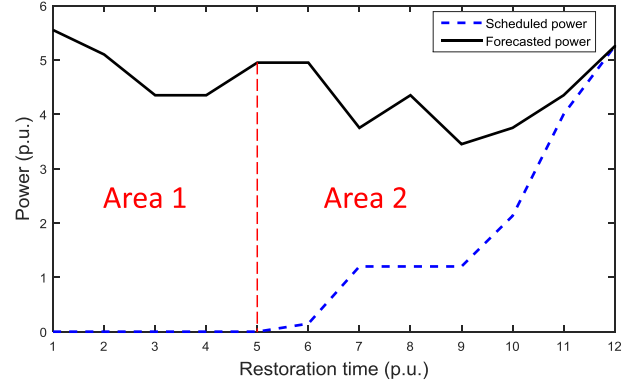
Fig. 3. Forecasted and scheduled wind farm output power without PSH contribution and wind uncertainty.
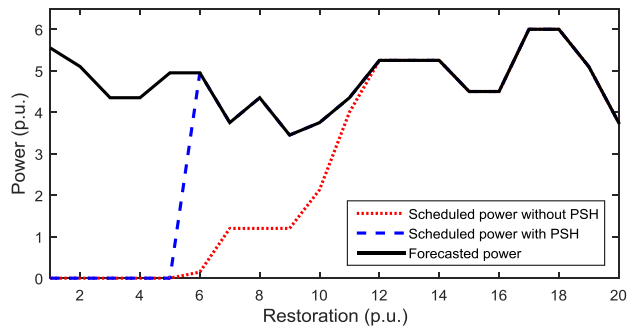
Fig. 4. Scheduled and forecasted wind farm output power with/without PSH units' contribution.

B. Wind-PSH Assisted Restoration

1) Restoration With PSH Contribution: First, we consider the participation of PSH units in the restoration process. Assume that the two PSH units are installed at bus 17, where the wind farm is located. Fig. 4 compares the scheduled wind power with/without PSH units' contribution. Note that wind uncertainty is not yet included (i.e., $\Delta_s = 0$). It can be seen that at restoration time $t = 6$, the scheduled wind power reaches its forecast. The total wind energy spillage reduces to 358.75 MWh, and the total energy severed increases to the 12.33 GWh. Small portion of wind power is used to serve loads and provide cranking power to other NBSUs, while the larger portion is used for pumping water to fill the upper reservoir. This helps to improve the total dynamic reserve level when a limited number of units are on. As the restoration process moves forward, more wind power can be accommodated into the system so that more capacities on NBSUs are released. As a result, the total load pickup capability of the system will be improved at later stages. Fig. 5 compares the load restoration curves with/without PSH units' contribution.

2) PSH Units' Location: The impact of PSH location is studied here. It is assumed that the PSH units are installed at bus 8. Note that in this scenario, although the wind farm becomes online after restoration time $t = 6$, the PSH units cannot store wind farm energy until $t = 9$. This is due to the fact that bus 8 is energized after $t = 9$, thus, imposing limitation on the operation of PSH units. Fig. 6 compares the reservoir volume for
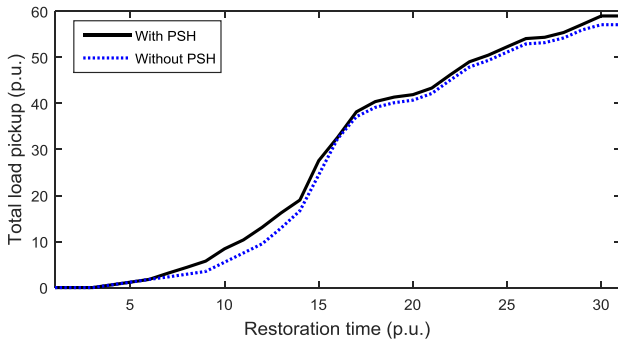
Fig. 5.   Total load pickup curves with/without PSH units' contribution.
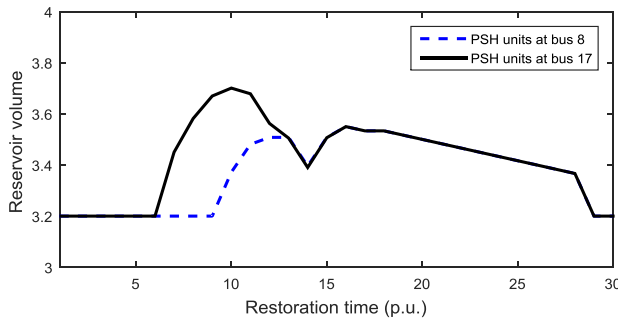
Fig. 6.   Reservoir volume (Hm^3) for different PSH locations.
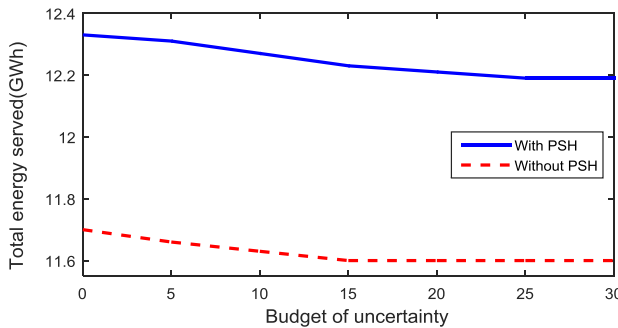
Fig. 7.   Impact of budget of uncertainty on total energy served with/without PSH units' contribution.

Fig. 8.   Scheduled and forecasted wind farm output power with/without PSH units' contribution including wind power fluctuations.

Fig. 9.   Impact of budget of uncertainty on total energy served with/without PSH units' contribution including wind power fluctuations.

different PSH locations. It can be seen that the pumping mode operation is postponed due to the unavailability of transmission path from $t = 6$ to $t = 9$. In this case, the total energy served is 12.163 GWh and total wind energy spillage is 542.74 MWh.

3) Wind Power Uncertainty: To model wind randomness in power system restoration, it is assumed that uncertain wind farm output power lies within the uncertainty set (1.27). The total restoration horizon in this study is set to 30 p.u., thus, the budget of uncertainty can vary within the interval [0, 30]. From Fig. 7, one can observe that when the budget of uncertainty increases, the total energy served will decrease in both scenarios. It also shows that with wind-PSH coordination the total energy served is always greater than that without PSH units. In particular, utilizing PSH units under the worst case conditions ($\Delta_s = 30$) outperforms the best case condition without PSH units, where $\Delta_s = 0$. Therefore, PSH units not only can compensate the wind uncertainty, but also facilitate load pickup.
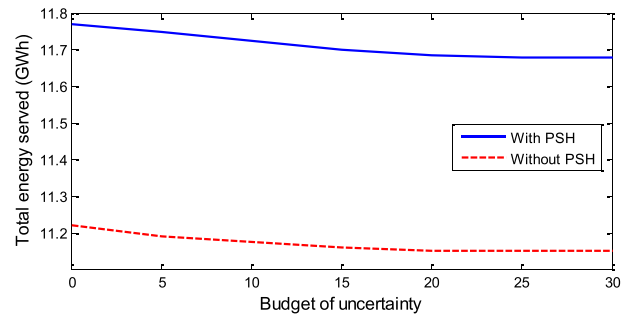
4) Wind Power Fluctuation: Now assume that wind power presents a large ramping behavior during the early stages of restoration between $t = 5$ and $t = 15$. Figs. 8 and 9 show that the PSH units are capable of handling large wind power fluctuations. Without PSH contribution, the wind power is curtailed to avoid load shedding and meet dynamic reserve requirement. However, coordinating with the PSH units, all wind energy can be harnessed despite the large fluctuations. The uncertainty study in Fig. 9 also demonstrates the effectiveness of PSH units in the event of high wind fluctuations. The PSH coordination consistently outperforms that without PSH units. The total energy served without PSH contribution is 11.22 GWh, whereas with PSH contribution it increases to 11.77 GWh; and total wind energy spillage reduces from 544.65 MWh to 332.50 MWh. It is worth noting that under wind power fluctuations and by utilizing PSH units, the total energy served becomes greater than the case where the wind power presents low fluctuations without utilizing PSH.

One should note that the level of conservatism of the optimal solution can be flexibly adjusted by setting the budget of uncertainty to a desired value. In fact, system operator should make a trade-off between the protection level of the constraint and the level of conservatism of the optimal solution. If the uncertainty is not considered, a large cost might be incurred once the uncertainty is revealed (e.g. load shedding might happen during the restoration period). Whereas, if the most conservative outcome of the uncertainty set is included in the model, the system is protected against the realizations that would be detrimental to
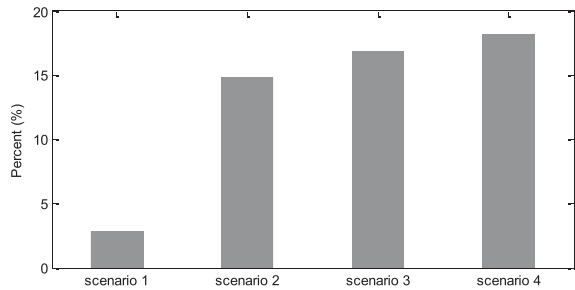
Fig. 10. Percentage of improvement in total energy served respect to the case where neither wind nor PSH units contributed to the restoration.

its security. However, the latter case is very unlikely to happen in practice and will definitely prolong the restoration time.

From Figs. 7 and 9, one can observe that if the budget of uncertainty increases (i.e., the level of conservatism increases), the objective function, reflecting the restoration performance, decreases. This happened as a result of incorporating uncertainty in the model yielding more robust solutions. It is worth noting that the objective function has not changed for $\Delta_s \geq 25$. This is due to the fact that wind farm started participating in the restoration process from $t > 5$. Thus, the uncertainty of wind power profile cannot influence the total energy served when $t < 5$, however, the total wind power spillage is impacted.

C. Impact of Wind Farm and Energy Storage

To further elaborate the impact of wind and energy storage on the restoration process, four scenarios have been defined as follows. Scenario 1: restoration with PSH units under minimum water level in the reservoir at $t = 0$. Scenario 2: restoration with PSH units under maximum water level in the reservoir at $t = 0$. Scenario 3: restoration with wind farm and PSH units under the overly conservative wind power and minimum water level in the reservoir at $t = 0$. Scenario 4: restoration with wind farm and PSH units without considering the wind uncertainty and with minimum water level in the reservoir at $t = 0$.

In Fig. 10, the percentage of increase in total energy served in each scenario is compared with the case where neither wind nor PSH contributed to the restoration process. As it can be seen from the figure, scenario 1 shows the lowest level of increase in the total energy served. That is, having PSH units with minimum level of water in the reservoir shows a negligible contribution respect to the other scenarios. This comes from the fact that at the initial stages of restoration, the conventional generation units devote their available capacities to pick up loads instead of pumping water and storing energy. Whereas, in scenario 2, one can observe the significant impact of PSH units when the reservoir has the maximum water level. In this scenario, PSH units work in generation mode for entire restoration time. Scenario 3 explicitly shows the impact of the wind when it is compared with scenario 1. Scenario 4 shows the maximum contribution of wind and PSH units under perfect forecast scenario.

Examining the results of Fig. 10 highlights the important role of the wind farm, particularly when water level in the upper reservoir reaches its minimum value right after the blackout incident. However, one should note that this paper assumed that

TABLE V
COMPARISON BETWEEN DIFFERENT APPROACHES

Study approach	Computation time (s)	Total energy served (GWh)
Deterministic(one-stage)	1464.5	12.33
Deterministic(two-stage)	187.2	12.33
Stochastic optimization	823.4	12.21
Proposed approach ($\Delta_s = 10$)	375.3	12.25
Proposed approach ($\Delta_s = 30$)	341.8	12.19

loads are fully dispatchable. If that is not the case (i.e., loads can only be picked up in blocks), as assumed and discussed in [11], the available generation might exceed the maximum amount of load that can be restored. In such cases, generation-load mismatch at each restoration period can pump water and store it in the upper reservoir. Consequently, PSH units present greater influence on the restoration process, regardless of the initial condition of water level in the reservoir.

D. Computational Performance and Comparison With Other Approaches

The performance of the robust optimization approach is demonstrated through comparison with the stochastic optimization method [29]. Stochastic optimization approach is the alternative approach to solve this problem; however, its main difficulty lies in the need to provide the probability distribution function of the forecast error, which is hard to obtain in real world. A normally distributed wind power prediction error with the standard deviation of 10% is assumed. Multiple scenarios are generated and an efficient scenario reduction algorithm is applied to produce a set of representative scenarios together with their associated probabilities. The objective function is minimized over all scenarios, weighing the value of each scenario in proportion to its probability.

Table V reports the computation time and total energy served; the latter reflects the objective function of restoration. It can be seen that, firstly, adopting the two-stage formulation with the proposed decomposition approach can notably reduce the computation time. Secondly, the stochastic optimization approach is computationally expensive compared with the robust optimization. Thirdly, after looking at the objective function of the robust optimization for different values of budget of uncertainty, one can see that this method provides the system operator a level of flexibility in choosing the trade-off between robustness and performance. For instance, if the trade-off is reached at $\Delta_s = 10$, the total energy served of the corresponding robust solution achieves increase of 0.48% over the solution obtained for $\Delta_s = 30$, and increase of 0.32% over the stochastic optimization solution.

V. CONCLUSION

This paper proposes a novel self-healing strategy by introducing wind-PSH coordination in restoration phase. Adaptive robust optimization approach was employed to solve the power system restoration problem under wind power uncertainty. Case study results showed that wind-PSH coordination can improve system load pickup capability through storing wind energy in the

initial phase of restoration and releasing it at final stages. Also, it was shown that the wind profile is a significant contributor to determine the total energy served and wind power spillage. In case of large wind power fluctuations, wind-PSH coordination enables system operators to harness more wind energy in initial stages of restoration. Besides, PSH units' location affects the total energy served through deferring the pumping time. The solution optimality is affected as the budget of uncertainty increases, but the wind-PSH coordination reduces the impact of wind uncertainty and improves its dispatchability. The proposed coordination strategy can be applied to the restoration problem both in transmission and distribution levels with conventional generators, renewable sources and energy storages.

The primary emphasis of future research on restoration topic is to further reduce our reliance on fossil fuel units, improve the renewable energy utilization, and shorten restoration time. To this end, our research directions include: 1) Development of real-time optimization tool for power system restoration by adopting other optimization techniques such as sliding window or distributed optimization and control approaches, 2) Study the impacts of utilizing renewable sources and energy storages as the black-start units and their capabilities to provide cranking power for conventional generators, 3) Integrate the differential/algebraic equation model of power system dynamics into the proposed adaptive robust optimization problem to specify the accurate size and location of the de-energized loads, and the dynamic reserve contribution of each generation unit.

APPENDIX
C&CG ALGORITHM

A. Inner-Level C&CG Algorithm for Identifying the Worst-Case Realization of Wind Uncertainty

The bi-level max–min problem (a.1) is a linear MIP in the inner minimization problem. Thus, it cannot be converted to a single level using Karush-Kuhn-Tucker (KKT) condition. An inner-level C&CG algorithm has been proposed to solve such problems and summarized as following steps:

$$\max_{\boldsymbol{\omega} \in \mathcal{W}} \min_{\boldsymbol{y}, \boldsymbol{z} \in \Omega(\hat{\boldsymbol{x}}, \boldsymbol{\omega})} \boldsymbol{b}^T \boldsymbol{y} \tag{a.1}$$

$$\text{s.t. } \boldsymbol{B}\boldsymbol{y} + \boldsymbol{Q}\boldsymbol{z} \leq \boldsymbol{g} - \boldsymbol{A}\hat{\boldsymbol{x}} - \boldsymbol{H}(\boldsymbol{\omega})\hat{\boldsymbol{x}} \; : \mu \tag{a.2}$$

Step 1: Set the upper and lower bounds of bi-level optimization problem (a.1)–(a.2) as $UB_i = \infty$ and $LB_i = -\infty$. Set the iteration count $k = 1$.

Step 2: With assigning an initial feasible value to binary variables vector $\hat{\boldsymbol{z}}^{(1)}$ and fixing the first-stage decision variable $\hat{\boldsymbol{x}}$, the inner minimization problem (a.1) becomes a LP problem that can be converted to a single-level optimization problem (a.3)–(a.9) using KKT conditions. Note that in (a.6)–(a.8), μ is dual variable of constraint (a.2), and constraints (a.7)–(a.8) are complementary slackness conditions which add non-linear terms to the constraints. However, binary variables and $Big - M$ method [16] can be used to linearize those constraints. After solving optimization problem (a.3)–(a.9), the worst case wind farm output power realization $\hat{\omega}^{(k)}$ is obtained and $UB_i = \hat{Q}(\hat{x})$

is updated. If $UB_i - LB_i \leq \epsilon$, return $\hat{\omega}^{(k)}$ and terminate.

$$Q(\hat{x}) = \max \alpha \tag{a.3}$$

$$\text{s.t. } \alpha \leq \boldsymbol{b}^T \boldsymbol{y}^{(v)} \; \forall 1 \leq v \leq k \tag{a.4}$$

$$\boldsymbol{B}\boldsymbol{y}^{(v)} \leq \boldsymbol{g} - \boldsymbol{A}\hat{\boldsymbol{x}} - \boldsymbol{H}(\boldsymbol{\omega})\hat{\boldsymbol{x}} - \boldsymbol{Q}\hat{\boldsymbol{z}}^{(v)} \; \forall 1 \leq v \leq k \tag{a.5}$$

$$\boldsymbol{B}^T \boldsymbol{\mu}^{(v)} \leq \boldsymbol{b}^T \; \forall 1 \leq v \leq k \tag{a.6}$$

$$\left(\boldsymbol{g} - \boldsymbol{A}\hat{\boldsymbol{x}} - \boldsymbol{H}(\boldsymbol{\omega})\hat{\boldsymbol{x}} - \boldsymbol{Q}\hat{\boldsymbol{z}}^{(v)} - \boldsymbol{B}\boldsymbol{y}^{(v)}\right).\boldsymbol{\mu}^{(v)} = 0 \; \forall 1 \leq v \leq k \tag{a.7}$$

$$\left(\boldsymbol{b}^T - \boldsymbol{B}^T \boldsymbol{\mu}^{(v)}\right).\boldsymbol{y}^{(v)} = 0 \tag{a.8}$$

$$\boldsymbol{\omega} \in \mathcal{W}, \boldsymbol{\mu}^{(v)} \leq 0, \; \boldsymbol{y} \in \mathbb{R}^p \; \forall 1 \leq v \leq k \tag{a.9}$$

Step 3: Having obtained $\hat{\omega}^{(k)}$ from (a.3)–(a.9), we solve optimization problem (a.10)–(a.11) to determine the lower bound of objective function (a.1). Update $LB_i = \max\{LB_i, \boldsymbol{b}^T \boldsymbol{y}^k\}$, if convergence tolerance $UB_i - LB_i \leq \epsilon$ is met, terminate and return $\hat{\omega}^{(k)}$.

$$\min_{\boldsymbol{y}, \boldsymbol{z} \in \Omega(\hat{\boldsymbol{x}}, \hat{\boldsymbol{\omega}}^{(k)})} \boldsymbol{b}^T \boldsymbol{y} \tag{a.10}$$

$$\text{s.t. } \boldsymbol{B}\boldsymbol{y} + \boldsymbol{Q}\boldsymbol{z} \leq \boldsymbol{g} - \boldsymbol{A}\hat{\boldsymbol{x}} - \boldsymbol{H}(\hat{\boldsymbol{\omega}})\hat{\boldsymbol{x}} \tag{a.11}$$

Step 4: Create new variables $(\boldsymbol{y}^{k+1}, \boldsymbol{\mu}^{(k+1)})$, and add the constraints (a-12)–(a.17) to optimization problem (a.3). In (a.13), $\hat{\boldsymbol{z}}^{(k+1)}$ is the optimal solution of $\hat{\boldsymbol{z}}$ at iteration k. Update $k = k + 1$ and go to step 2.

$$\alpha \leq \boldsymbol{b}^T \boldsymbol{y}^{(k+1)} \tag{a.12}$$

$$\boldsymbol{B}\boldsymbol{y}^{(k+1)} \leq \boldsymbol{g} - \boldsymbol{A}\hat{\boldsymbol{x}} - \boldsymbol{H}(\boldsymbol{\omega})\hat{\boldsymbol{x}} - \boldsymbol{Q}\hat{\boldsymbol{z}}^{(k+1)} \tag{a.13}$$

$$\boldsymbol{B}^T \boldsymbol{\mu}^{(k+1)} \leq \boldsymbol{b}^T \tag{a.14}$$

$$\left(\boldsymbol{g} - \boldsymbol{A}\hat{\boldsymbol{x}} - \boldsymbol{H}(\boldsymbol{\omega})\hat{\boldsymbol{x}} - \boldsymbol{Q}\hat{\boldsymbol{z}}^{(k+1)} - \boldsymbol{B}\boldsymbol{y}^{(k+1)}\right).\boldsymbol{\mu}^{(k+1)} = 0 \tag{a.15}$$

$$\left(\boldsymbol{b}^T - \boldsymbol{B}^T \boldsymbol{\mu}^{(k+1)}\right).\boldsymbol{y}^{(k+1)} = 0 \tag{a.16}$$

$$\boldsymbol{\omega} \in \mathcal{W}, \boldsymbol{\mu}^{(k+1)} \leq 0, \; \boldsymbol{y} \in \mathbb{R}^p \tag{a.17}$$

B. Outer-Level C&CG Algorithm for Solving Master Problem

We adopt outer C&CG algorithm to solve the master problem so as to determine the optimal solution in the first-stage, including the on time of generation units and energization times of transmission lines and buses. The outer C&CG algorithm is described as follows:

Step 1: Set $UB_o = \infty$ and $LB_o = -\infty$, and iteration count $k = 1$.

Step 2: Solve the master problem (b.1)–(b.4) and derive the optimal solution $(\hat{\boldsymbol{x}}^{(k)}, \hat{\varphi}^{(k)})$ and update $LB_o = \boldsymbol{c}^T \hat{\boldsymbol{x}}^{(k)} + \hat{\varphi}^{(k)}$.

If $UB_o - LB_o \leq \epsilon$, return $\hat{\boldsymbol{x}}^{(k)}$, $\hat{\boldsymbol{y}}^{(k)}$, $\hat{\boldsymbol{z}}^{(k)}$ and terminate.

$$\min_{\boldsymbol{x}, \boldsymbol{y}, \boldsymbol{z}} \boldsymbol{c}^T \boldsymbol{x} + \varphi \tag{b.1}$$

$$\text{s.t.} \ \ \varphi \geq \boldsymbol{b}^T \boldsymbol{y}^{(l)} \ \forall 1 \leq l \leq k \tag{b.2}$$

$$\boldsymbol{F}\boldsymbol{x} \leq \boldsymbol{f} \tag{b.3}$$

$$\boldsymbol{A}\boldsymbol{x} + \boldsymbol{B}\boldsymbol{y}^{(l)} + \boldsymbol{H}(\hat{\boldsymbol{\omega}}^{(l)})\boldsymbol{x} + \boldsymbol{Q}\boldsymbol{z}^{(l)} \leq \boldsymbol{g} \ \forall 1 \leq l \leq k \tag{b.4}$$

Step 3: Call inner-level C&CG algorithm to obtain optimal value of $Q(\hat{x}^{(k)})$ and update $UB_o = \min\{UB_o, \boldsymbol{c}^T \hat{\boldsymbol{x}}^{(k)} + Q(\hat{x}^{(k)})\}$. If $UB_o - LB_o \leq \epsilon$, terminate the algorithm and return $\hat{\boldsymbol{x}}^{(k)}$, $\hat{\boldsymbol{y}}^{(k)}$, and $\hat{\boldsymbol{z}}^{(k)}$.

Step 4: Create new variables $(y^{(k+1)}, z^{(k+1)})$ and add constraints (b.5)-(b.6) to master problem (b.1). Update $k = k + 1$, and go to step 2.

$$\varphi \geq \boldsymbol{b}^T \boldsymbol{y}^{(k+1)} \tag{b.5}$$

$$\boldsymbol{A}\boldsymbol{x} + \boldsymbol{B}\boldsymbol{y}^{(k+1)} + \boldsymbol{H}(\hat{\boldsymbol{\omega}}^{(k+1)})\boldsymbol{x} + \boldsymbol{Q}\boldsymbol{z}^{(k+1)} \leq \boldsymbol{g} \tag{b.6}$$

REFERENCES

[1] L. Fried, S. Sawyer, S. Shukla, and L. Qiao, "Global wind report: Annual market update 2012," [Online]. Available: http://www.gwec.net/wp–content/uploads/2012/06/Annual_report_2012_LowRes.pdf

[2] U.S. Department of Energy, "20% wind energy by 2030." 2008. [Online]. Available: http://www.eere.energy.gov/windandhydro/pdfs/41869.pdf

[3] U.S. Department of Energy, "Wind Vision: A new era for wind power in the United States." 2015. [Online]. Available: https://www.energy.gov/sites/prod/files/2015/03/f20/wv_full_report.pdf

[4] N. Li and K. W. Hedman, "Economic assessment of energy storage in systems with high levels of renewable resources," *IEEE Trans. Sustain. Energy*, vol. 6, no. 3, pp. 1103–1111, Jul. 2015.

[5] M. Amin and A. Giacomoni, "Smart grid, safe grid," *IEEE Power Energy Mag.*, vol. 10, no. 1, pp. 33–40, Jan./Feb. 2012.

[6] H. Zhu and Y. Liu, "Aspects of power system restoration considering wind farms," in *Proc. Int. Conf. Sustain. Power Generation Supply*, Sep. 2012, pp. 1–5.

[7] M. Aktarujjaman, M. A. Kashem, M. Negnevitsky, and G. Ledwich, "Black start with DFIG based distributed generation after major emergencies," in *Proc. Int. Conf. Power Electron., Drives Energy Syst.*, Dec. 2006, pp. 1–6.

[8] L. Seca, H. Costa, C. L. Moreira, and J. A. Lopes, "An innovative strategy for power system restoration using utility scale wind parks," in *Proc. Bulk Power Syst. Dyn. Control-IX Optimization, Security Control Emerging Power Grid*, Aug. 2013, pp. 1–8.

[9] A. M. El-Zonkoly, "Renewable energy sources for complete optimal power system black-start restoration," *IET Gener. Transmiss. Distrib.*, vol. 9, no. 6, pp. 531–539, Apr. 2015.

[10] S. M. Mohammadi-Hosseininejad, A. Fereidunian, A. Shashavari, and H. Lesani, "A healer reinforcement approach to self-healing in smart grid by PHEVs parking lot allocation," *IEEE Trans. Ind. Informat.*, vol. 12, no. 6, pp. 2020–2030, Dec. 2016.

[11] A. Golshani, W. Sun, and Q. Zhou, "PHEVs contribution to the self-Healing process of distribution systems," in *Proc. IEEE PES Gen. Meeting*, Jul. 2016, pp. 1–5.

[12] C. P. Nguyen and A. J. Flueck, "Agent based restoration with distributed energy storage support in smart grids," *IEEE Trans. Smart Grid*, vol. 3, no. 2, pp. 1029–1038, Jun. 2012.

[13] H. Weber and M. Krueger, "Dynamic investigation of network restoration by the pumped-storage plant Markersbach in Germany," in *Proc. 17th IFAC World Congr.*, 2008, pp. 7004–7009.

[14] R. Jiang, J. Wang, and Y. Guan, "Robust unit commitment with wind power and pumped storage hydro," *IEEE Trans. Power Syst.*, vol. 27, no. 2, pp. 800–810, May 2012.

[15] M. E. Khodayar, M. Shahidehpour, and L. Wu, "Enhancing the dispatchability of variable wind generation by coordination with pumped-storage hydro units in stochastic power systems," *IEEE Trans. Power Syst.*, vol. 28, no. 3, pp. 2808–2818, Aug. 2013.

[16] W. Sun and A. Golshani, "Harnessing renewables in power system restoration," presented at the Conf. IEEE PES General Meeting, Denver, CO, USA, Jul. 26–30, 2015.

[17] A. L. Soyster, "Convex programming with set-inclusive constraints and applications to inexact linear programming," *Oper. Res.*, vol. 11, pp. 1154–1157, 1973.

[18] A. Ben-Tal and A. Nemirovski, "Robust convex optimization," *Math. Oper. Res.*, vol. 23, pp. 769–805, 1998.

[19] C. Zhao, J. Wang, J. P. Watson, and Y. Guan, "Multi-stage robust unit commitment considering wind and demand response uncertainties," *IEEE Trans. Power Syst.*, vol. 28, no. 3, pp. 2708–2717, Aug. 2013.

[20] D. Bertsimas, E. Litvinov, X. Sun, J. Zhao, and T. Zheng, "Adaptive robust optimization for the security constrained unit commitment problem," *IEEE Trans. Power Syst.*, vol. 28, no. 1, pp. 52–63, Feb. 2013.

[21] B. Hu and L. Wu, "Robust SCUC considering continuous/discrete uncertainties and quick-start units: A two-stage robust optimization with mixed-integer recourse," *IEEE Trans. Power Syst.*, vol. 31, no. 2, pp. 1407–1419, Mar. 2016.

[22] B. Zeng and L. Zhao, "Solving two-stage robust optimization using a column-and-constraint generation method," *Oper. Res. Lett.*, vol. 41, no. 5, pp. 457–461, Sep. 2013.

[23] M. M. Adibi and L. H. Fink, "Special considerations in power system restoration," *IEEE Trans. Power Syst.*, vol. 7, no. 4, pp. 1419–1427, Nov. 1992.

[24] A. Golshani, W. Sun, Q. Zhou, Q. P. Zheng, and J. Tong, "Two-stage adaptive restoration decision support system for a self-healing power grid," *IEEE Trans. Ind. Informat.*, vol. 13, no. 6, pp. 2802–2812, Dec. 2017.

[25] P. A. Trodden, W. A. Bukhsh, A. Grothey, and K. I. M. McKinnon, "Optimization-based islanding of power networks using piecewise linear AC power flow," *IEEE Trans. Power Syst.*, vol. 29, no. 3, pp. 1212–1220, May 2014.

[26] PJM Manual 36: System Restoration. 2013. [Online]. Available: https://www.pjm.com/documents/manuals.aspx

[27] A. J. Conejo, J. M. Arroyo, J. Contreras, and F. A. Villamor, "Self-scheduling of a hydro producer in a pool-based electricity market," *IEEE Trans. Power Syst.*, vol. 17, no. 4, pp. 1265–1272, Nov. 2002.

[28] IEEE 39 Bus System, Illinois Center for a Smarter Electric Grid (ICSEG). [Online]. Available: http://publish.illinois.edu/smartergrid/ieee

[29] F. Bouffard and F. D. Galiana, "Stochastic security for operations planning with significant wind power generation," *IEEE Trans. Power Syst.*, vol. 23, no. 2, pp. 306–316, May 2008.